Mon. Not. R. Astron. Soc. **000**, 000–000 (0000) Printed 5 February 2008 (MN LATEX style file v2.2)

Planets and Asteroids in the γ Cephei system

P. E. Verrier⋆ and N. W. Evans⋆
Institute of Astronomy, University of Cambridge, Madingley Road, Cambridge, CB3 0HA, United Kingdom

5 February 2008

ABSTRACT
The binary star system γ Cephei is unusual in that it harbours a stable giant planet around the larger star at a distance only about a tenth of that of the stellar separation. Numerical simulations are carried out into the stability of test particles in the system. This provides possible locations for additional planets and asteroids. To this end, the region interior to the planet is investigated in detail and found to permit structured belts of particles. The region between the planet and the secondary star however shows almost no stability. The existence of an Edgeworth-Kuiper belt analogue is found to be a possibility beyond 65 au from the barycentre of the system, although it shows almost no structural features. Finally, the region around the secondary star is studied for the first time. Here, a zone of stability is seen out to 1.5 au for a range of inclinations. In addition, a ten Jupiter-mass planet is shown to remain stable about this smaller star, with the habitability and observational properties of such an object being discussed.

Key words: stars: individual: γ Cephei (HR 8974) – planetary systems – binaries: general – methods: N-body simulations

1 INTRODUCTION

γ Cephei is one of the closest separation binary systems that contains a planet. The primary and secondary stars are separated by 18.5 au. The planet (designated γ Cep Ab) has a minimum mass of 1.7 $M_{\rm J}$ and follows an eccentric orbit about the larger star alone. The observational parameters of γ Cephei, as determined by Hatzes et al. (2003), are summarised in Table 1.

Although the data are reasonably reliable, there is some uncertainty regarding the masses of the components. The inclination to the line of sight of a spectroscopic binary is usually indeterminate. This means that the mass of the primary is generally reckoned from spectral type. Then, the mass function (e.g., Smart 1977) permits a minimum mass to be assigned to the secondary, albeit crudely (Griffin, Carquillat & Ginestet 2002).

For γ Cephei, the mass of the primary is $\approx 1.57 M_\odot$ from photospheric modelling (Fuhrmann 2004). The most recent determination from stellar evolution models is $\approx 1.7 M_\odot$ (Affer et al. 2005). The mass of the secondary is given by Dvorak et al. (2003) as $\approx 0.4 M_\odot$. However, assuming the original value of the primary's mass of 1.57 $M_\odot$, a minimum mass can be derived as ≈ 0.34 $M_\odot$ from the velocity amplitude fitted by Hatzes et al. (2003).

There have been a number of studies of the dynamics of the γ Cephei system to date. Foremost is the numerical investigation of Dvorak et al. (2003), which does use an earlier, and slightly different, set of orbital parameters (see Table 2). They used Burlisch-Stoer and Fast Liapunov Indicator methods to show that the γ Cephei system is stable over Myr time-scales. They carried out test particle integrations as a guide to the possible existence of further planets. The results show a stable inner region between 0.5 and 0.8 au and then an additional stable zone at low inclination around 1 au. Dvorak et al. (2003) noted that this coincides with the 3:1 mean motion resonance. This resonance is stable in the γ Cephei system, but is unstable in the Solar system. Dvorak et al. (2003) conclude that Earth-mass planets (up to 90 $M_{\rm E}$) can exist in this region which is fortunately just on the edge of the habitable zone [1]. An extension to this work by Dvorak et al. (2004) showed that the planet's eccentricity is less important than that of the two stars for the stability of a second planet. Haghighipour (2005) also carried out numerical studies of the system's stability using a Burlisch-Stoer integrator, for a range of possible configurations of the planet's and binary's semimajor axes, eccentricities and inclinations, confirming and extending the results of Dvorak et al. (2003).

Here, we use both numerical simulations and analytic calculations to study zones of stability as possible locations of additional planetary companions to either star and asteroid or Edgeworth-Kuiper belt analogues. Edgeworth-Kuiper belts are of particular interest in binary systems, as they may be being observed (indirectly) in exosystems such as τ Ceti and η Corvi (Greaves et al. 2004; Wyatt et al. 2005). The results fall into three categories: possible planetary companions and asteroid belts centred on the primary star (§2), planetary companions around the secondary star (§3) and finally possible Edgeworth-Kuiper belt about both stars (§4).

⋆ E-mail: pverrier@ast.cam.ac.uk (PEV); nwe@ast.cam.ac.uk (NWE)

[1] The habitable zone has boundaries which depend on assumptions regarding stellar luminosity and effective temperature, as well as the climate model adopted for the hypothetical habitable planet.

Name	γ Cep A	γ Cep B	γ Cep Ab
Class	K1IV sub-giant star	M dwarf star	Planet
Mass	$1.59 \pm 0.12\ M_\odot$	$0.4\ M_\odot$	$1.7 \pm 0.4\ M_J$
Period (days)	–	20750.6579 ± 1568.6	905.574 ± 3.08
Semimajor axis (au)	–	18.5 ± 1.1	2.13 ± 0.05
Eccentricity	–	0.361 ± 0.023	0.12 ± 0.05
Longitude of periastron (°)	–	158.76 ± 1.2	49.6 ± 25.6
Time of periastron passage (JD)	–	2448429.03 ± 27.0	2453121.925 ± 66.9

Table 1. Best fit orbital parameters for the γ Cephei system from Hatzes et al. (2003). Mass of star B is from Dvorak et al. (2003).

Name	γ Cep A	γ Cep B	γ Cep Ab
Class	K1IV sub-giant star	M dwarf star	Planet
Mass	$1.6M_\odot$	$0.4M_\odot$	$1.76M_J$
Period (days)	–	25567.5	902.2
Semimajor axis (au)	–	21.36	2.15
Eccentricity	–	0.44	0.209

Table 2. Orbital parameters for the γ Cephei system used by Dvorak et al. (2003).

2 PLANETS AND ASTEROID BELTS AROUND THE PRIMARY

2.1 Algorithm

For all the simulations, we use the parameters of the γ Cephei system given in Table 1. Here and elsewhere in the paper, the equations of motion are integrated using a conservative Burlisch-Stoer method provided in the `MERCURY` software package (Chambers 1999). Although not as fast as sympletic methods, this was chosen because of its ability to provide close encounter data and handle highly eccentric objects. The two stars and planet are simulated as point masses for gravitational interactions. Any additional objects are taken as massless test particles to decrease integration times. Test particles are removed from the simulations when they collide with the primary star, or pass an ejection distance of the order of several hundred au. A collision with the primary means that the test particle has a position that lies within the body of the primary, as judged by its stellar radius of 0.02 au (Hatzes et al. 2003). Close encounters are allowed to occur, and are defined as taking place whenever a test particle enters within one Hill radius $R_{\rm H}$ of the secondary star or the planet, defined as

$$R_{\rm H} = a\left(\frac{m}{3M}\right)^{1/3} \quad (1)$$

where m is the mass of the secondary or planet and M is the mass of the primary. This works out as ≈ 8.1 au for the secondary and ≈ 0.15 au for the planet.

To maintain accuracy, the variation in the system's total energy and angular momentum is monitored throughout each simulation. Using this to constrain the initial timestep to 1 day and the tolerance in the Burlisch-Stoer algorithm (Press et al. 1999) to 10^{-12} leads to an overall fractional change in the system's energy $\Delta E/E$ of about 10^{-8} over a 100 Myr period. This can therefore be considered the maximum time the system can be accurately followed. All the simulations presented here are typically 1 Myr in time-scale, for which $\Delta E/E \approx 10^{-11}$ or better.

It is straightforward to show that the γ Cephei system has long term stability. A 100 Myr integration shows no major variation in the orbits. Regular short period variations do occur, for example, a slight oscillation of the planet's semimajor axis over timescales equal to both its orbital period and the binary's orbital period. An additional secular variation is seen over a period of about 5500 years, evident in the eccentricity and longitude of the planet only. This secular period is in good agreement with the results of quadrupole theory (see eq. (36) of Ford et al. (2000)).

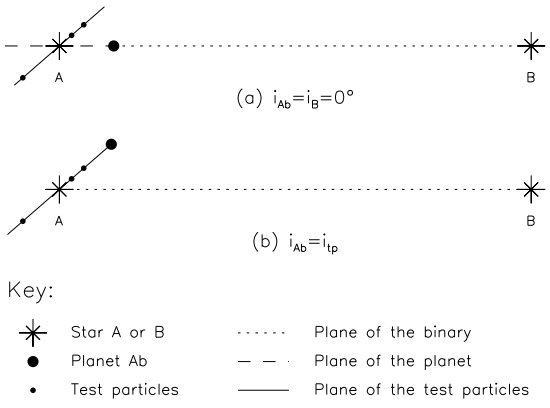

Figure 1. Two possible configurations for test particles. Top: the planet remains in the plane of the binary and the test particles are inclined relative to this. In other words, the inclination of the planet $i_{\rm Ab}$ is the same as the inclination of the secondary $i_{\rm B}$ and both are zero. Bottom: the planet and test particles have the same inclination relative to the plane of the binary. In other words, $i_{\rm Ab}$ is equal to the inclination of the test particles $i_{\rm tp}$.

2.2 Test Particles Interior to the Orbit of the Planet

Figure 1 shows two possible configurations of test particles in the system considered here. In the first, the test particles are inclined to the common plane of the binary and planet. In the second, both the test particles and planet are coplanar, yet inclined relative to the plane of the binary. The binary is always assumed to be viewed edge-on (that is, it lies in a plane perpendicular to the plane of the sky). If the planet is at an inclination $i_{\rm Ab}$ relative to this, its mass must be increased accordingly by dividing by $\sin i$ where $i = 90° - i_{\rm Ab}$.

With the planet and binary coplanar, we begin by investigating the stability of test particles in the region interior to the known planet. A grid of particles with semimajor axis from 0.5 to 1.85 au and inclination from 0° to 50° with resolution 0.05 au and 5° respectively is integrated for 1 Myr. Thirty-six particles are started at each grid point with varying initial longitudes of pericentre ($\omega = 0°, 60°, \ldots 300°$) and longitudes of ascending node ($\Omega = 0°, 60°, \ldots 300°$). The orbits are initially circular. The stability is then determined by computing the mean survival time $\langle t_{\rm s} \rangle$ in Myrs at each grid point averaged over the 36 test particles. The results are shown in Figure 2 and can be compared to figure 2 of

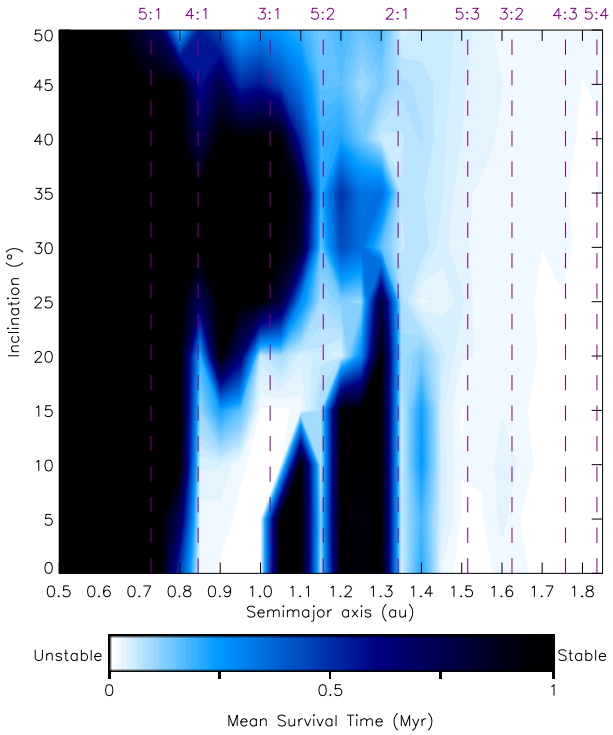

Figure 2. Stability map for test particles interior to the orbit of the planet in the coplanar case $i_{Ab} = 0$. Here, stability is indicated by the test particle's survival time averaged over longitudes and normalised to 1 Myr. Darker colours indicate more stable regions, whilst lighter colours show less stable regions. Over-plotted in purple are the nominal locations of the mean motion resonances with the planet Ab, up to the 5:4 case.

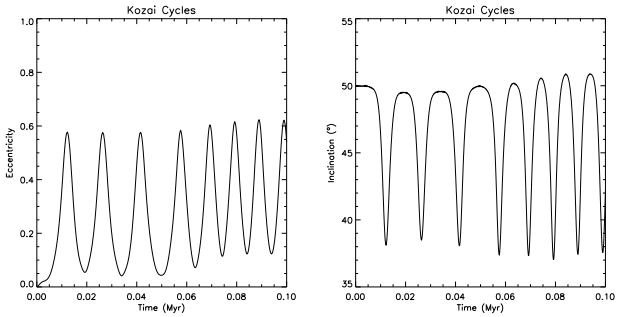

Figure 3. The variation of eccentricity and inclination with time for a test particle undergoing Kozai cycles. The starting elements are $a = 0.5$ au and $i = 50°$.

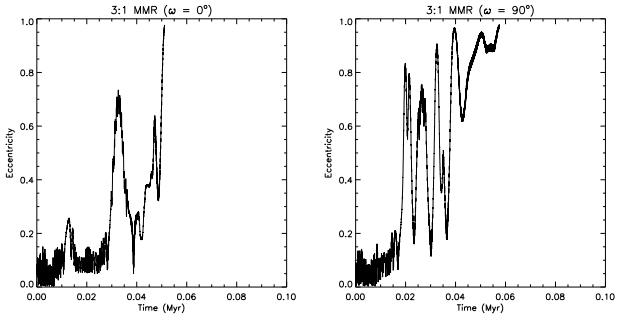

Figure 4. The variation of eccentricity with time for test particles at the 3:1 MMR for starting $\omega = 0°$ and 90°.

Dvorak et al. (2003). Note that our stability index is slightly different to the criteria used by Dvorak et al. (2003), who removed test particles after they become orbit crossing. This may miss the occasional test particle that is stable, for example, if it lies in a Trojan-like orbit. We only remove test particles if they collide with the central star or are ejected from the system.

The map shows test particles with semimajor axes less than ≈ 1.4 au are stable. However, there is a strip of instability between roughly 0.8 and 1.0 au, creating an island of stability at low inclinations between 1.0 and 1.3 au. Some of the structure in the map can be clearly related to the positions of the mean motion resonances (MMRs) with the planet (indicated in Fig. 2). The 4:1, 3:1, 5:2 and 2:1 resonances seem to mark transitions from stability to instability. For example, the 5:2 MMR divides the island at ≈ 1.15 au. The lack of effect of some of the higher order MMRs, such as the 5:1 case, is probably due to their comparative weakness and narrowness. The lack of stability beyond ≈ 1.4 au is readily explained. The gravitational reach of the planet as a multiple of the Hill radius (Jones, Underwood & Sleep 2005) places the limit on stability at 1.31 au, a good match with the results here. Note that in calculating this limit the maximum eccentricity of the planet obtained during the simulation has been used. Many of the test particles in the high inclination region of Figure 2 show evidence of Kozai cycles, as illustrated by the orbits in Figure 3. The Kozai (1962) instability is well-known from studies of high inclination comets and asteroids in the Solar system. It sets in at inclinations greater than a critical value of $i_{\rm crit} = \text{asin}\sqrt{0.4} \approx 39.23°$. During Kozai cycles, the eccentricity and inclination vary so as to maintain approximate constancy of the integral of motion $I_{\rm K} = \sqrt{1-e_{\rm tp}^2}\cos i_{\rm tp}$, where $e_{\rm tp}$ is the test particle's eccentricity. As the semimajor axis increases, the amplitude of eccentricity and inclination librations becomes larger, thus accounting for the increased instability evident in this region of Figure 2.

As already seen, the MMRs with the planet are important in shaping the regions of stability. However, one major feature unexplained by this is the instability strip between roughly 0.8 and 1.0 au. Although at zero inclination the edges are marked by the 4:1 and 3:1 MMRs, the instability strip shows a pronounced evolution with inclination which is suggestive of a secular resonance instead. The classical Laplace-Lagrange linear theory (Murray & Dermott 2000), although derived for low eccentricity and inclination regimes around a dominant central mass, can be applied to give a first approximation of the locations of these resonances. A secular resonance for a test particle occurs when its precession rate has exactly the same magnitude as an eigenfrequency of the system. The eigenfrequencies are easily calculable for the three body system made up of the two stars and planet and are the eigenvalues of the 2x2 matrices **A** and **B** respectively, which have components

$$\begin{aligned} A_{jj} &= +n_j \frac{1}{4}\frac{m_k}{M+m_j}\alpha\bar{\alpha}b^{(1)}_{3/2}(\alpha), \\ A_{jk} &= -n_j \frac{1}{4}\frac{m_k}{M+m_j}\alpha\bar{\alpha}b^{(2)}_{3/2}(\alpha), \\ B_{jj} &= -A_{jj}, \\ B_{jk} &= -A_{jk}\frac{b^{(1)}_{3/2}(\alpha)}{b^{(2)}_{3/2}(\alpha)}. \end{aligned} \quad (2)$$

Here, n_j is the mean motion of object j (1 represents the planet and 2 represents the secondary), m_j and a_j are the mass and semimajor axis of object j, M is the mass of the primary (the central object), $\alpha = a_1/a_2$ and $b^{(1)}_{3/2}(\alpha)$ and $b^{(2)}_{3/2}(\alpha)$ are Laplace coefficients. Using the values for the masses and semimajor axes given in Table 1 along with $n_1 = 145.2^\circ$ yr^{-1}, $n_2 = 6.337^\circ$ yr^{-1} and $\alpha = 0.1151$ gives the Laplace coefficients as $b^{(1)}_{3/2}(\alpha) = 0.3542^\circ$ yr^{-1} and $b^{(2)}_{3/2}(\alpha) = 0.05089^\circ$ yr^{-1}, employing the `MATHEMATICA` routines of Murray & Dermott (2000). Calculating the matrices and solving for the eigenfrequencies gives

$$\begin{aligned} g_1 &= 0.04338^\circ \text{ yr}^{-1}, \\ g_2 &= 0.00005211^\circ \text{ yr}^{-1}, \\ f &= -0.04343^\circ \text{ yr}^{-1}, \end{aligned} \tag{3}$$

where g_1 and g_2 are the eigenvalues of $\mathbf{A}$ and f is the degenerate eigenvalue of $\mathbf{B}$. Note that the g_1 and f eigenfrequencies have about the same magnitude, whilst g_2 is almost zero due to the large mass ratio between the planet and secondary star. The precession rate of the test particle is given by

$$A_{\rm tp} = n\frac{1}{4}\left(\frac{m_1}{M}\alpha_1\bar{\alpha}_1 b^{(1)}_{3/2}(\alpha_1) + \frac{m_2}{M}\alpha_2\bar{\alpha}_2 b^{(1)}_{3/2}(\alpha_2)\right) \tag{4}$$

where n is the particle's mean motion. For the region interior to the planet $\alpha_j = \bar{\alpha}_j = a/a_j$, where a is the test particles semimajor axis. Plotting $A_{\rm tp}$ as a function of a from 0.5 to 1.85 au shows a resonant location where the g_1 and f eigenfrequencies intersect the curve at $\approx$ 0.8 au. This supports the idea that the location of the inner edge of the instability strip on the map coincides with a secular resonance.

Comparing our results with those of Dvorak et al. (2003), it is easy to see that the broad trends are similar, despite slightly differing orbital elements. The main stable regions are slightly closer to the star in Dvorak et al. (2003). This may be due to a higher eccentricity of both the planet and the secondary, which means that they approach the central star more closely, reducing separations with the test particles. Dvorak et al. (2003) find that the 3:1 MMR is stable, in contrast to asteroids in the Solar System in the same resonance with Jupiter. Here, we find that the resonance is unstable, with a particle following a fairly steady evolution until switching to a mode where its eccentricity is rapidly driven to unity on a time-scale of 10 kyrs, as shown in Figure 4.

The case where the planet is also inclined ($i_{Ab} \neq 0$) has not been previously studied. This is a more likely configuration for a system that has formed in a common protoplanetary disc. Here, we investigate this case by using the same grid of test particles as before, but with the planet sharing the same inclination as the test particles and with $\Omega_{Ab} = 0$. This means that, to reproduce the same radial velocity dataset, the mass of the planet must be increased by dividing by $\sin i$, where $i = 90^\circ - i_{Ab}$.

The results are displayed in Figure 5. As compared to the earlier case of Figure 2, the unstable region has expanded, especially at high inclinations. This is partly caused by the change in the extent of the gravitational reach of the planet, as shown by the dotted curve in Figure 5. Although this does scale with the increasing planetary mass, the sharp change at 40° inclination is due to the planet becoming subject to Kozai cycles. The large increase in eccentricity here means that the planet's periastron is much closer to the star, and hence its gravitational influence is larger. At 50°, the planet is unstable, colliding with the central star after $\approx$ 0.5 Myr.

At first sight, it may seem that the rest of the increased instability evident in Figure 5 is caused by the increased mass of the planet. However, experiments show that this is not so. For example,

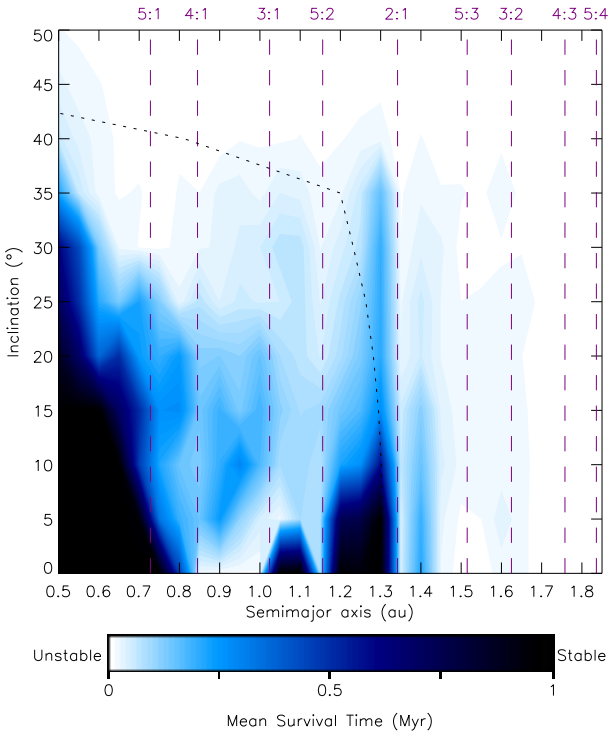

Figure 5. As Figure 2, but here the planet and test particles are all inclined to the plane of the binary. Over-plotted in purple are the nominal locations of the mean motion resonances with the planet Ab, up to the 5:4 case. The dotted curve shows the gravitational reach of the planet, calculated using the method of Jones et al. (2005).

an integration of the 30° case with the planet inclined but at minimum mass ($1.7M_J$) shows very little difference to Figure 5. This suggests that the cause lies in the relative inclination of test particle and planet to the plane of the binary. In the case of Figure 2, the amplitude of libration of $i_{\rm tp}$ and $e_{\rm tp}$ of test particles is generally modest for all cases below $i_{\rm crit}$, the critical value for the Kozai instability. For test particles in Figure 5, the amplitude is no longer small and becomes larger with increasing inclination, rapidly driving particles into the regime where the Kozai instability is effective. This is understandable as in the former case, the forces due to the masses in the system are always directed towards the plane of the binary, whereas in the latter case this is not true. As the inclination increases, the misalignment between the forces due to the stars and the force due to the planet increases, and so the amplitude of libration increases.

2.3 Test Particles Interior to the Orbit of the Binary

Holman & Wiegert (1999) have already studied the stability of test particles in binary systems. These may orbit either a single star or both stars. Here, we study test particles around the primary star. For this case, Holman & Wiegert (1999) introduced the notion of a critical semimajor axis $a_{\rm crit}$, which is the largest circular orbit around the primary for which a ring of test particles survives for at least 10^4 binary periods ($\approx$ 600 kyrs in the case of γ Cephei). Using their eq (1), we find $a_{\rm crit} = 4.0 \pm 0.6$ au. In other words, our expectation is that all test particles starting out at semimajor axes greater than 4.0 au will be rapidly swept out. The existence of the

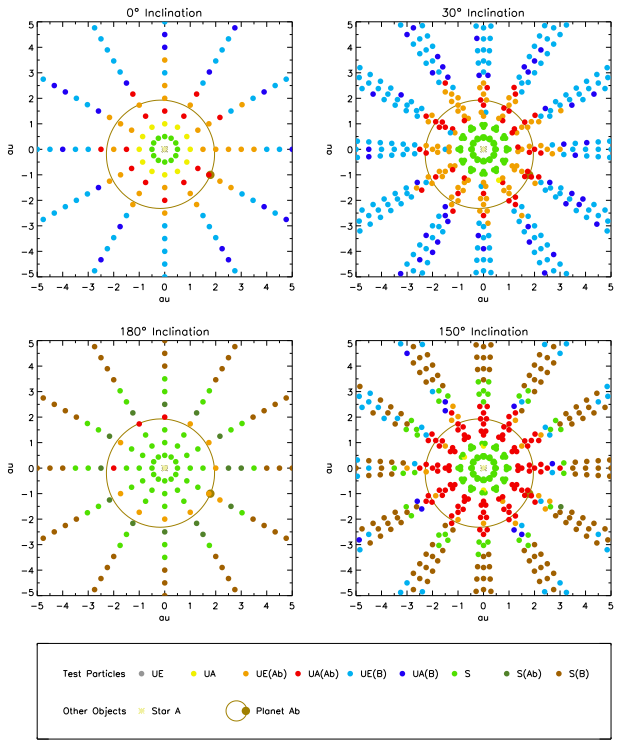

Figure 6. The ultimate fate of test particles interior to the orbit of the binary, with inclinations $0°, 30°, 150°$ and $180°$. For clarity, only test particles in and above the plane of the binary and planet are displayed. The following abbreviations are used in the key: UE = unstable, ejected from the system; UA = unstable, collided with star A; UE(Ab) = unstable, ejected from the system after a close encounter with Ab; UA(Ab) = unstable, collided with A after a close encounter with Ab; UE(B) = unstable, ejected from the system after a close encounter with B; UA(B) = unstable, collided with star A after a close encounter with B; S = stable; S(Ab) = stable, but suffered a close encounter with Ab; S(B) = stable, but suffered a close encounter with B.

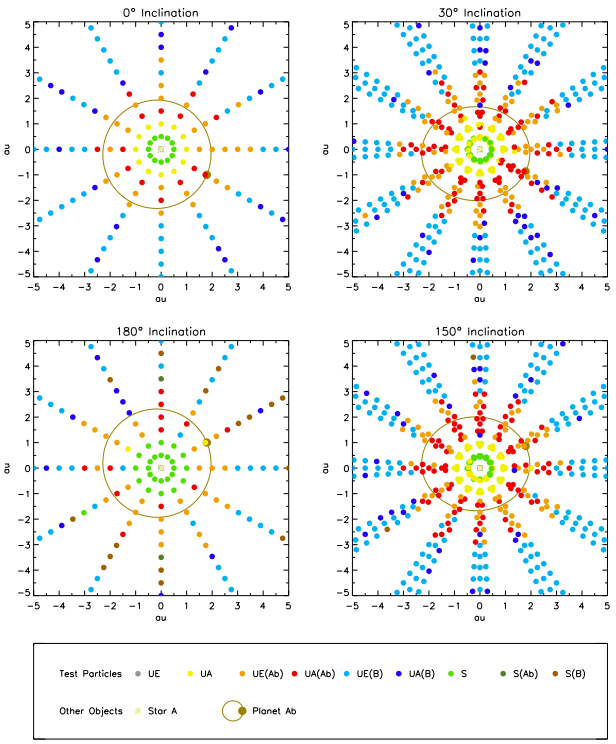

Figure 7. As Figure 6, but the test particles and the planet are similarly inclined.

comparatively large and eccentric planet γ Cephei Ab will cause further de-stabilization.

To investigate this, simulations of test particles in the region from 0.5 to 20.0 au are carried out. They have initially zero eccentricity and are set up on a grid with resolution 0.5 au in starting semimajor axis. The range of inclinations is restricted from $0°$ to $30°$ for the prograde case, and from $150°$ to $180°$ for the retrograde case, both in steps of $10°$. Seventy-two particles are started at each grid point with varying initial longitudes of pericentre ($\omega = 0°, 30°, \ldots 330°$) and longitudes of ascending node ($\Omega = 0°, 60°, \ldots 300°$). The orbits of the test particles are followed for 1 Myr, and any close encounters are recorded. Although this is a limited range of inclinations, it is expected that those not investigated are largely unstable. This receives confirmation from exploration integrations in the case of $70°$ inclination, for which very few test particles survive throughout the entire region.

Figures 6 and 7 show the ultimate fates of the test particles within 5 au. They differ in that the planet is in the plane of the binary and test particles are inclined in Figure 6, whilst both planet and test particles are similarly inclined in Figure 7. Four panels showing the results of selected simulations are displayed in each case, corresponding to prograde with $i_{\rm tp} = 0°$ and $30°$, retrograde with $i_{\rm tp} = 180°$ and $150°$.

In the inner regions, test particles close to the planet are swept out on a precession time-scale ($\approx$ 5.5 kyrs). Within $\approx$ 3 au, prograde test particles are either ejected or collide with the central star after a close encounter with the planet. This is evident from the particles coloured orange and red in the upper panels of both Figures 6 and 7. The retrograde case is different. The lower panels of Figure 6 show swathes of stable particles coloured either brown or green, according to whether they reside within the Hill sphere of the secondary or not. Note that the secondary's periastron is at 11.8 au, so particles out to 3.7 au are within its Hill sphere at some point. In the case $i_{\rm tp} = 180°$, the retrograde stability zone extends out to $\approx$ 7 au. As the inclination decreases ($i_{\rm tp} \rightarrow 150°$), the stability zone shrinks to the annuli between 0.5 to 1.0 au and 3.0 to 5.0 au. The lower panels of Figure 7 show the case when both test particles and planet are retrograde. In the case $i_{\rm tp} = 180°$, the large stability region seen previously has almost completely disappeared. There are only a few remaining test particles that survive the 1 Myr integration. The similarity of the two right-hand panels of this figure shows that the inner region's evolution is almost entirely controlled by the planet.

The numbers of test particles surviving after 1 Myr at each semimajor axis are given in Table 3. Shown in Figure 8 are the mean survival times plotted against semimajor axis for a variety of inclinations. The mean survival time $\langle t_{\rm s} \rangle$ can be computed by averaging over the results for the differing longitudes of ascending node and pericentre at fixed semimajor axis and inclination. The averaging is over 12 test particles for $i_{\rm tp} = 0°$ and $180°$ and 72 for all other cases. Test particles that survive to the end of the integrations are included with a survival time of 1 Myr, so that the computed mean survival time is a lower limit in these cases. Figure 8 shows that there is a region of enhanced stability with $\langle t_{\rm s} \rangle \approx 100$ kyrs – for all the studied inclinations – centred at $\approx$ 3.5 au, just beyond the

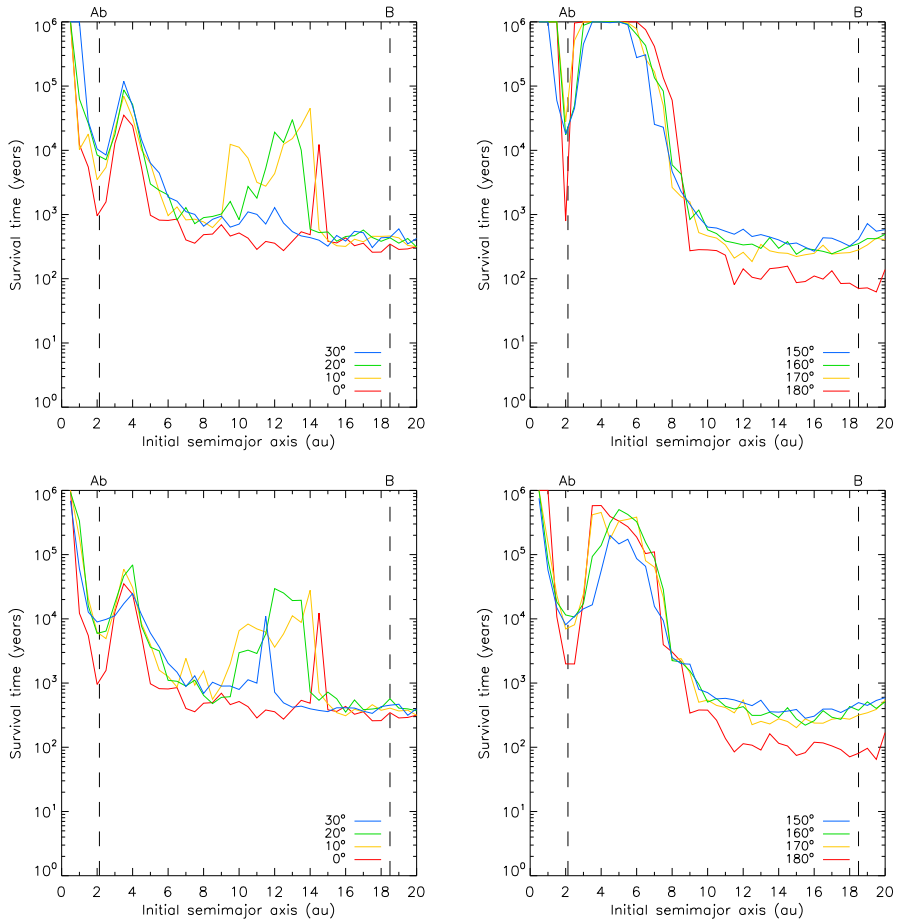

Figure 8. The mean survival time of test particles as a function of starting semimajor axis for particles interior to the orbit of the binary. In the left-hand panels, the starting inclination of the test particles is 0° (red), 10° (yellow), 20° (green) and 30° (blue); in the right-hand panels, it is 180° (red), 170° (yellow), 160° (green) and 150° (blue). The top panels are inclined test particles only, the bottom panels are similarly inclined test particles and planet. The starting semimajor axis of the secondary star and the planet are shown as vertical dashed lines.

Table 3. The number of test particles interior to the orbit of the binary at each starting semimajor axis and inclination that survive for 1 Myrs. There are 72 test particles initially for all cases except $i = 0°$ and $i = 180°$, which have 12.

	Starting Semimajor Axis [in au]																			
Inclination	0.5	1.0	1.5	2.0	2.5	3.0	3.5	4.0	4.5	5.0	5.5	6.0	6.5	7.0	7.5	12.0	12.5	13.0	13.5	14.0
0°	12	-	-	-	-	-	-	-	-	-	-	-	-	-	-	-	-	-	-	-
10°	72	-	-	-	-	-	-	-	-	-	-	-	-	-	-	-	-	-	-	2
20°	72	-	-	-	-	-	-	-	-	-	-	-	-	-	-	1	-	2	-	-
30°	72	72	-	-	-	-	-	-	-	-	-	-	-	-	-	-	-	-	-	-
150°	72	67	-	-	-	23	72	70	67	72	60	11	14	-	-	-	-	-	-	-
160°	72	72	72	-	-	54	72	72	72	72	62	39	25	3	1	-	-	-	-	-
170°	72	72	72	-	24	72	72	72	72	72	68	49	15	4	1	-	-	-	-	-
180°	12	12	12	-	11	12	12	12	12	12	12	12	8	4	1	-	-	-	-	-
0°	12	-	-	-	-	-	-	-	-	-	-	-	-	-	-	-	-	-	-	-
10°	72	-	-	-	-	-	-	-	-	-	-	-	-	-	-	-	-	-	-	-
20°	60	17	-	-	-	-	1	2	-	-	-	-	-	-	-	1	-	1	1	-
30°	35	-	-	-	-	-	-	-	-	-	-	-	-	-	-	-	-	-	-	-
150°	37	-	-	-	-	-	-	-	5	-	1	-	-	-	-	-	-	-	-	-
160°	69	-	-	-	-	-	2	1	10	13	15	10	4	1	-	-	-	-	-	-
170°	72	-	-	-	-	-	25	16	4	9	11	11	-	-	-	-	-	-	-	-
180°	12	12	-	-	-	-	6	5	4	2	2	-	-	-	-	-	-	-	-	-

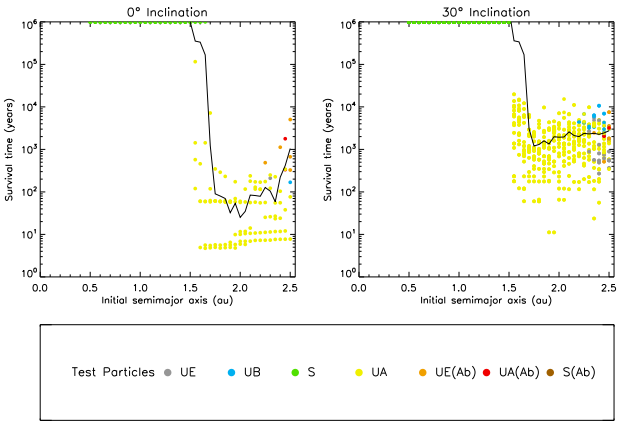

Figure 9. The mean survival times (black line) and fate of individual particles (coloured points) for test particles around star B. The results are shown for inclinations 0° and 30°. The fate of each particle is given by the key: UE = unstable, ejected from the system; UB = unstable, collided with star B; S = stable; UA = unstable, collided with star A; UE(Ab) = unstable, ejected from the system after a close encounter with Ab; UA(Ab) = unstable, collided with star A after a close encounter with Ab; S(Ab)= stable, but suffered a close encounter with Ab. Note that, in the retrograde cases, almost all particles are stable for the length of the integration (1 Myr).

gravitational reach of the planet but within the critical semimajor axis and just within the region affected by the secondary. Most test particles here (and also beyond this region) suffer a close encounter with the secondary before ejection or collision with the primary. The effect of the secondary star becomes increasingly important with increasing semimajor axis and $\langle t_s \rangle$ falls to ≈ 1 kyr. There is, for the prograde cases, a region of enhanced stability around 12 au for some inclinations, clearly visible in Figure 8. This is due to a few particles surviving here for the full length of the integration.

As stated in the introduction, the mass of star B is uncertain. By altering this parameter and rerunning some of the simulations the importance of the uncertainty can be seen. For the coplanar configuration of test particles described in this section, changing the mass of star B by $\sim 20\%$ results in almost no difference in global statistical properties, such as average survival times. This would indicate that the system's dynamics are not significantly affected by the uncertainty in the secondaries mass.

3 PLANETS AND ASTEROID BELTS AROUND THE SECONDARY

Here, we investigate whether planets could exist around star B. This possibility has not been investigated before for this system. The critical semimajor axis for stability, as defined by Holman & Wiegert (1999), is 1.9 ± 1.0 au. To investigate further, test particles are set up from 0.5 to 2.5 au in steps of 0.05 au for inclinations 0° to 30° and 150° to 180° in steps of 10°. The particles are on initially circular orbits again, and spaced in longitude of perihelion and ascending node by 60° as before. The results of two of the prograde cases are shown in Figure 9. Prograde test particles are not stable beyond 1.5 au. In the case of 10°, 20° and 30° inclinations, the unstable test particles generally survive at least ten times longer than those in the 0° case. The unstable test particles within about 2 au all collide with the primary, whilst those beyond this point have a range of fates. Holman & Wiegert's critical semimajor axis

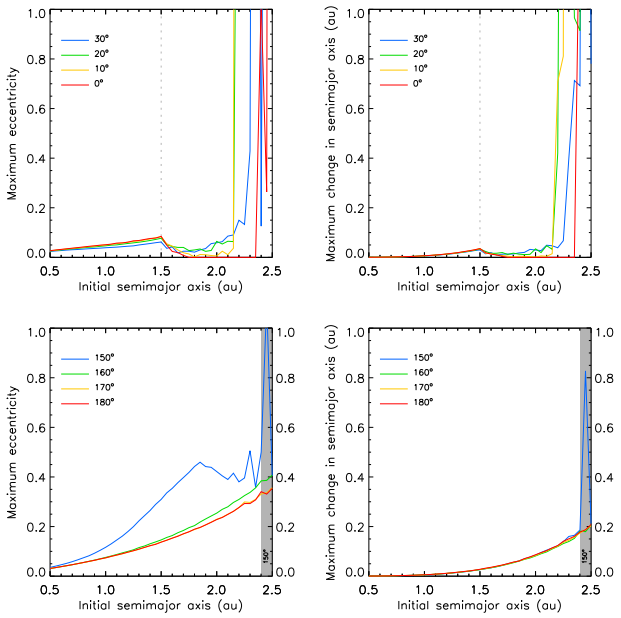

Figure 10. The average maximum eccentricity and maximum change in semimajor axis for test particles around star B. This is calculated by averaging over longitude at each semimajor axis. The inclinations shown in the top panels are: 0° (red), 10° (yellow), 20° (green) and 30° (blue). The inclinations shown in the bottom panels are 180° (red), 170° (yellow), 160° (green) and 150° (blue). Also shown as dashed vertical lines are the semimajor axis within which all particles remain stable. For the 150° case the one unstable semimajor axis is shaded in grey.

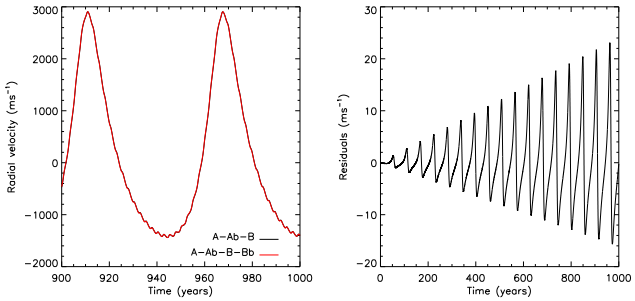

Figure 11. The radial velocity curve (left) and residuals (right) for the primary star when there is an additional planetary companion to star B. The additional planet has a mass of $10M_J$. The radial velocity curve shows the original system in black and the new two planet system in red. The residuals are calculated by subtracting these two curves. When there is no planet around star B the star has an increased mass of $M_B + M_{Bb}$, where M_{Bb} is the mass of the additional planet to be added to the later simulation.

does not match up as well as in Section 2.3, but still agrees within the rather large uncertainty. In the retrograde cases, almost all the test particles are stable, with the exception of 7 particles at 2.45 au in the 150° case. Integrating more distant particles shows that the retrograde stability reaches out to about 3.5 au.

The stability of the test particles can be further investigated by plotting the evolution of their eccentricity and semimajor axis, as shown in Figure 10. For all the simulations, there is not much change in the inclination of the test particles. The variation in eccentricity and semimajor axis of stable particles increases as the initial distance from star B increases, and is similar for all the pro-

grade cases. However, the variation is much larger for the (more stable) retrograde cases. When $i_{\rm tp} = 150°$, the variations are no longer smoothly increasing and show abrupt jumps, indicating that this case may not be long term stable.

As test particles can remain stable around the secondary, this raises the question of whether a massive planet could also persist here. So, it is interesting to consider whether this could be detectable in the radial velocity curve of the primary star. To investigate this, the simple case of a 10 Jupiter-mass planet in a coplanar, circular orbit with initial semimajor axis 0.5 au and initial longitude 0° is integrated. The orbital elements of the secondary are adjusted so that the centre of mass of it and its putative planet orbits the primary with the elements shown in Table 1 for star B alone. As expected from the test particle results, the planet remains stable for the full Myr length of the integration and shows very little variation in its orbit. However, the 1 Myr integrations here may overestimate the extent of the stability zone for planets, as instabilities can appear even after 100 Myr of apparent stability (Jones, Sleep & Chambers 2001). To calculate the radial velocity curve, the system is assumed to be at zero inclination relative to the line of sight ($i = 90°$). Figure 11 shows the radial velocity curve of the primary, together with the residuals with respect to the case with no extra planet. There is no detectable signal with the period of the extra planet. The small variations shown, which have the period of the binary, amount to 25 $\rm ms^{-1}$ over 1000 yr timespans, would be undetectable.

4 EDGEWORTH-KUIPER BELT ANALOGUES

The final region remaining to be studied is that exterior to the binary. This may host particles analogous to the Edgeworth-Kuiper belt in our own Solar system. There is observational evidence for the existence of extrasolar Edgeworth-Kuiper belts from infrared imaging of dusty discs around other stars (e.g., Wyatt 2003, Greaves et al. 2004), so the longevity of such a structure around γ Cephei is worth investigation.

Numerical integrations of test particles around binary systems suggest that they will remain stable in this region (e.g., Harrington 1977). In addition to the criterion in Section 2.3, Holman & Wiegert (1999) also provide an empirical rule-of-thumb to determine prograde test particle stability exterior to the binary. Here, the critical semimajor axis $a_{\rm crit}$ is that beyond which almost all test particles survive for at least 10^4 binary periods. Using eq. (3) of their paper, we find that $a_{\rm crit} = 64 \pm 2$ au. However, Holman & Wiegert (1999) caution that there can sometimes be islands of instability beyond the critical radius associated with n:1 MMRs. There is an older criterion due to Harrington (1977), who also considers the case of retrograde test particles. Harrington's equation suggests that prograde test particles are stable for $a \gtrsim 56$ au and retrograde stable for $a \gtrsim 45$ au. By stability, Harrington means that the particles show bounded motion with no secular or large periodic variations in their elements over his – by nowadays standards – very small integration timespans. Using the same method as in Sections 2.2 and 2.3, test particles are set up with inclinations 0 to 30° and 150° to 180° in the (barycentric) region from 20 to 150 au in steps of 5 au. The mean survival times are shown in Figure 12. The prograde test particles exhibit a sharp cut-off, with those beyond 65 au being stable, independent of the starting inclination. This figure also shows that the retrograde test particles survive to the end of the integration for starting semimajor axes beyond 40 au for 180° inclination, 45 au for 170° and 160° inclinations and 60 au for 150° inclination. The range of initial conditions for which retrograde particles survive is larger than for prograde (e.g., Harrington 1977). For all inclinations, unstable particles from about 20 to 40 au are removed quickly and generally are ejected after a close encounter with the secondary. Unstable particles from about 40 to 65 au are less rapidly removed and tend to collide with star A or be ejected from the system, without experiencing a prior close encounter. We see that both Harrington's (1977) and Holman & Wiegert's (1999) stability criteria seem to give a reasonable description of the results of our simulations.

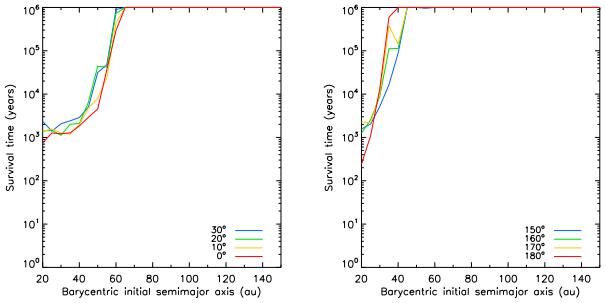

Figure 12. Average survival time of test particles exterior to the binary as a function of barycentric initial semimajor axis. In the left hand panel the starting inclinations are: 0° (red), 10° (yellow), 20° (green) and 30° (blue). In the right hand panel the starting inclinations are: 180° (red), 170° (yellow), 160° (green) and 150° (blue).

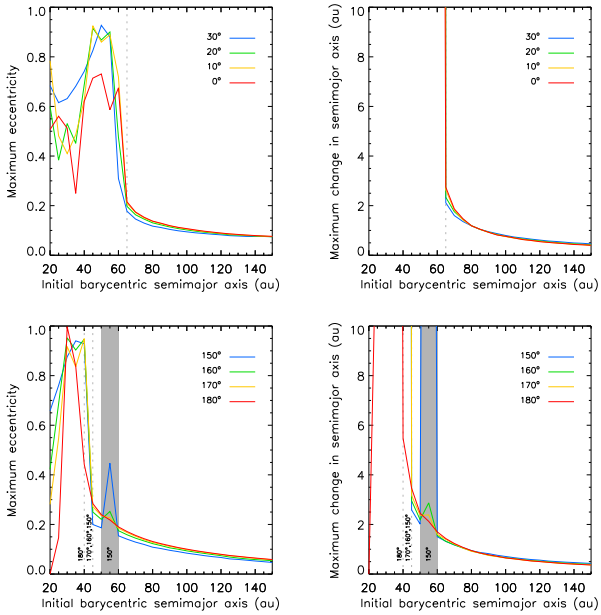

Figure 13. The average maximum eccentricity and maximum change in semimajor axis of each test particle in the region exterior to the binary, as a function of starting semimajor axis. The inclinations shown are as for Figure 12, and the averages calculated as for Figure 10. The boundaries between the unstable and stable regions are shown as dashed grey lines. An isolated unstable region is shown as a shaded area for the 150° case, as in Figure 10.

The average maximum eccentricity and change in semimajor axis is shown in Figure 13 as a function of initial semimajor axis for all eight inclinations. All the test particles show a small secular variation in their orbital elements.

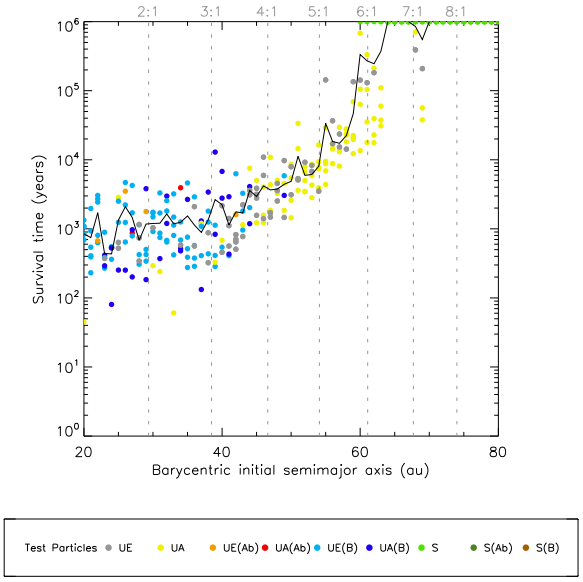

Figure 14. The average survival times (black line) and fate of individual particles (coloured points) for test particles in the region exterior to the binary. This is for an inclination of 0° and with a resolution of 1 au in semimajor axis. Only the particles out to 80 au are shown, as the simulation is stable beyond here. The locations of the *n*:1 MMRs are shown as dashed grey lines and labelled above the plot. The colour coded fates of test particles are as in Figure 6.

The Edgeworth-Kuiper belt in our Solar system shows some structure due to locations of MMRs with the giant planets (e.g., Luu & Jewitt 2002). However, the results in Figure 12 do not indicate any such resonant features. This is most likely due to the coarse semimajor axis grid employed. To investigate this, the coplanar case was re-run, but now with a spacing in semimajor axis of 1 au. The mean survival times and fates of individual particles for this simulation are shown in Figure 14. The first location where all test particles survive is now 64 au, agreeing exactly with Holman & Wiegert's value of $a_{\rm crit}$. There is then an unstable band from 67 to 70 au that seems to match up to the 7:1 MMR. The plot gives no evidence for any other resonant effects beyond this location. This is understandable since the locations of the other major resonances are outside the region of Hill stability (for example, the 3:2 resonance that is important in our own Solar system), leaving only those of very high order to affect stable test particles. The distinct difference in fates of test particles is obvious in this plot, with the blue coloured points, indicating close encounters with star B, not occurring beyond about 45 au. At this point, the test particles are yellow or grey, indicating either ejection or collision with star A without undergoing any close encounter.

5 CONCLUSIONS

In this paper, we have carried out a suite of test particle integrations for the γ Cephei system, as a guide to possible locations for additional planets. For test particles in the plane of the binary and planet, there are three zones of stability for 1 Myr timespans at least. These are [1] the region interior to the planet, which is stable within the bands 1.2 and 1.3 au, 1.05 to 1.15 au, and 0.75 to at least 0.5 au, [2] the region around star B from 1.5 au into at least 0.5 au and [3] the region around both stars extending out from about 65 au. These can be used to constrain possible locations of additional planetary companions.

The region interior to the planet has a complicated structure. Low order resonances, such as the 4:1, 3:1 and 5:2, mark transitions between stable and unstable regimes. There is a secular resonance located at 0.8 au from the primary that also plays a role in the dynamics of the test particles. The results for this region match up well with the previous work of Dvorak et al. (2003) despite the differences in the parameters of the system and the methods used. This implies that the slight improvements in the observations of the system have not significantly altered its dynamical characteristics. One difference though is that, unlike Dvorak et al. (2003), we find that test particles close to the 3:1 resonance are unstable, just as for the asteroid belt in the Solar System. In agreement with Dvorak et al. (2003), we find that small planets interior to γ Cephei Ab are long-lived. Another as yet unconsidered possibility seen from the results here is the existence of an asteroid belt interior to the giant planet. However, the stability seen for test particles in this region disappears when γ Cephei Ab is inclined in the same plane as the test particles. Now, the test particles are rapidly driven to inclinations which are subject to the Kozai instability.

The region interior to the binary and exterior to the planet is unpromising. It seems unlikely that any prograde planet or asteroid can remain stable between γ Cephei Ab and the binary, although retrograde test particles in this region are more long-lived. The region around the secondary is stable out to 1.5 au for test particles. We have shown that planets up to 10 Jupiter-masses in circular orbits at 0.5 au can survive for at least 1 Myr. This seems to be a promising place for additional planets to reside, in a similar manner to satellites about a planet around a single star.

In the final region, that exterior to the binary, test particles are also stable. Although planets would be able to reside out here, the existence of an Edgeworth-Kuiper belt structure is also a possibility. Once again the retrograde particles are more stable than those that are prograde. Whilst in every region studied this is true, such objects are perhaps unlikely, if the origin of the system was a common disk. If particles are captured from elsewhere, then this may become a possibility. Retrograde asteroids and comets certainly exist in the Solar system.

Since the survival of additional planets in the system has been shown to be a possibility, it is interesting to consider their habitability. There are a number of estimates of the habitable zone around star A in the literature. For example, Dvorak et al. (2003) place it at 1.0 to 2.2 au, in which case habitable planets could exist at the very edge of the zone. However, Haghighipour (2005) places the habitable zone at 3.1 to 3.8 au, while Jones et al. (2005) place it at 2.07 to 4.17 au. These different locations reflect differences in the criteria for the location of the habitable zone or the assumed stellar luminosity and effective temperature. The zone 2.07 to 4.17 au is unstable for all except retrograde test particles. So, this would permit the possibility of a habitable planet only if retrograde. The detection of any such small planet is challenging, given the small (of the order of a few $\rm ms^{-1}$) radial velocity signatures that they cause. In addition, a retrograde planet appears in radial velocity curves merely as a prograde one with a 180° phase difference. Although retrograde objects – especially planets – are thought to be unlikely, it has been shown that giant planets in binary systems can end up with retrograde orbits after close encounters within a planetary system (Marzari et al. 2005).

A more interesting possibility is that of a habitable planet around star B, since it has been shown that planets can survive

here. Theories of planetary formation do not preclude this possibility (e.g., Armitage, Clarke & Palla 2003). The habitable zone for an M dwarf extends out to about 0.3 au (Kasting, Whitmire & Reynolds 1993), which is within the stable zone found here. The large primary star nearby might also act as a 'shield' from comets and asteroids similar to Jupiter for the Earth. As seen in the results in Sections 3 and 4, very few test particles collide with the secondary star once the region interior to the binary has been rapidly cleared. Edgeworth-Kuiper belt objects that are perturbed into the inner regions of the system are also likely to suffer encounters with the primary, thus leaving the secondary and its environs largely unscathed.

The detection of such a habitable planet around star B has, unfortunately, been shown to be virtually impossible from the radial velocity signature of star A alone. Should the secondary be resolved this would change, and any companion giant planet would be easily detectable. The region around star B, none the less, remains as a promising place for the existence of a habitable planet in this system.

ACKNOWLEDGMENTS

PEV acknowledges financial support from the Particle Physics and Astronomy Research Council. We thank the referee for his helpful report.

REFERENCES

Affer L., Micela G., Morek T., Sanz-Forcada J., Favata F. 2005, A&A, 433, 647
Armitage P. J., Clarke C. J., Palla F. 2003, MNRAS, 342, 1139
Chambers J. 1999, MNRAS, 304, 793
Dvorak R., Pilat-Lohinger E., Funk B., Freistetter F. 2003, A&A, 398, L1
Dvorak, R., Pilat-Lohinger, E., Bois, E., Funk, B., Freistetter, F., Kiseleva-Eggleton, L. 2004, Revista Mexicana de Astronomia y Astrofisica Conference Series, 21, 222
Greaves J. S., Wyatt M. C., Holland W. S., Dent W. R. F. 2004, MNRAS, 351, L54
Ford, E. B., Kozinsky, B., Rasio, F. A. 2000, ApJ, 535, 385
Fuhrmann K., 2004, Astron. Nach., 325, 3
Griffin, R. F., Carquillat, J.-M., Ginestet, N. 2002, The Observatory, 122, 90
Hatzes A.P., Cochran W.D., Endl M., McArthur B., Paulson D. B., Walker G.A.H., Campbell B., Yang S. 2003, ApJ, 599, 1383
Haghighipour N. 2005, ApJ, submitted (astro-ph/0509659)
Harrington R.S. 1977, AJ, 82, 753
Holman, M. J., & Wiegert, P. A. 1999, AJ, 117, 621
Jones B. W., Sleep P. N., Chambers, J. E. 2001, A&A, 366, 254
Jones B. W., Underwood D. R., Sleep P. N. 2005, ApJ, 622, 1091
Kasting J. F., Whitmire D. P., Reynolds R. T. 1993, Icarus, 101, 108
Kozai, Y. 1962, AJ, 67, 591
Luu J. X., Jewitt D. C. 2002, ARAA, 40, 63
Marzari F., Weidenschilling S. J., Barbieri M., Granata V. 2005, ApJ, 618, 502
Murray C. D., Dermott S. F. 2000, Solar System Dynamics, Cambridge University Press, chap. 7
Press W.H., Flannery B.P., Teukolsky S.A., Vetterling W.T. 1999, Numerical Recipes, Cambridge University Press, Cambridge
Smart W.M. 1977, Spherical Astronomy, chap 14
Wyatt M. C., Holland W. S., Greaves J. S., Dent W. R. F. 2003, Earth Moon and Planets, 92, 423
Wyatt M. C., Greaves J. S., Dent W. R. F., Coulson I. M. 2005, ApJ, 620, 492